

Influence of Interfacial Compliance on Thermomechanical Stresses in Multilayered Microelectronic Packaging

Cemal Basaran and Yujun Wen

Abstract—Many analytical procedures are proposed for thermomechanical analysis of layered structures, mostly based on the perfectly bonded interfacial conditions. However, in the microelectronics industry, there is a strong desire to design packages with flexible interfaces to decrease interfacial stresses and interfacial delamination. In this paper, an analytical model based on flexible interfacial compliances is presented for multilayered microelectronic structures where loading can be a thermal gradient across the layers rather than uniform temperature. Interfacial stresses and the normal stresses in the layers can be calculated very efficiently and quickly compared to time-consuming finite-element analysis and following asymptotic analysis. The influence of interfacial compliance on thermomechanical stresses is investigated for different cases.

Index Terms—Adhesive, delamination, electronic packaging, laminated substrate.

I. INTRODUCTION

MATERIALS with different coefficients of thermal expansion (CTE) and stiffness are bonded together to form laminated stacks in microelectronic packaging. Thermal stresses, usually causing interfacial delamination and crack in silicon die, result from the CTE mismatch of the adhesively joined materials. Predicting the thermal stresses in multilayered microelectronic packaging is always a challenging task. This problem is particularly severe during manufacturing stage of semiconductor devices.

Many researchers studied the failure mechanisms in multilayered structures. Timoshenko [5] is the first one to study the interlaminar stresses in layered structures. An extensive survey on the subject is presented in the earlier papers by the authors.

The biggest drawback of most of the proposed analytical methods is that they were not verified in the laboratory, especially for small-scale structures like microelectronics. Another drawback of the analytical solutions is that they assume a uniform temperature change (isothermal condition) across the structure. In most microelectronics, there is a gradient of temperature across the package, not a homogeneous field. Moreover, most of the models proposed in the literature assume rigid interfaces and isotropic material properties. Wen and

Manuscript received October 17, 2003; revised September 16, 2004. This work was supported in part by the National Science Foundation under Grant CMS 9908016 and in part by ONR Advanced Electrical Power Systems under the supervision of Program Director T. Ericson.

C. Basaran is with the Electronic Packaging Laboratory, State University of New York, Buffalo, NY 14260 USA (e-mail: cjb@buffalo.edu).

Y. Wen is with Shanghai Shentong Holdings Company, Ltd., Shanghai, China.

Digital Object Identifier 10.1109/TADVP.2006.871175

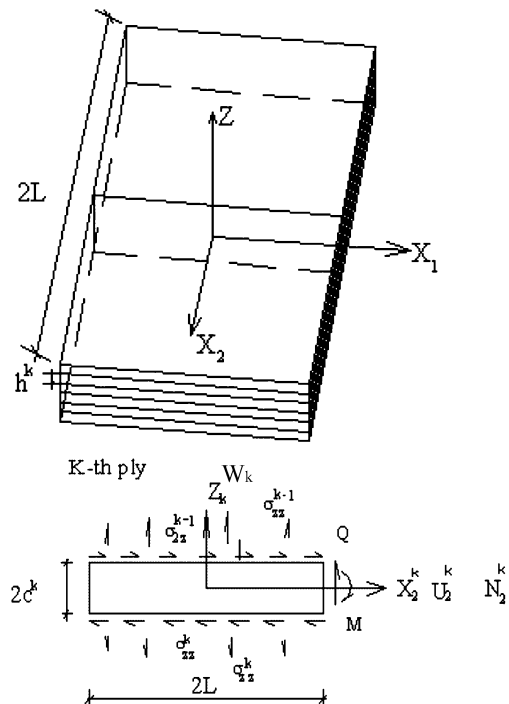


Fig. 1. Generic laminated beam-type plate with compliant interfaces.

Basaran [7], [8] developed an analytical model for multilayered microelectronic structures based on the refined plate theory with the assumption of perfectly bounded interfaces and homogeneous thermal field. This model considers each layer as a beam-type plate with orthotropic material properties. Wen and Basaran analytical solution was verified in the laboratory by using high-sensitivity moiré interferometry. In this paper, the interfacial compliances and temperature gradient are introduced into the model and the influence of interfacial compliances on the thermomechanical stresses is investigated for different cases.

II. FORMULATION OF THE ANALYTICAL MODEL

Consider N -layer laminated plate with compliant interfaces as shown in Fig. 1.

Assuming there are no body forces and couple stresses acting on the system, for a beam-type plate force and moment equilibrium equations for a k th layer can be given by

$$N_{2,2}^k + n_2^k = 0 \quad (1)$$

$$M_{2,2}^k + c_k m_2^k - Q_2^k = 0 \quad (2)$$

$$Q_{2,2}^k + q^k = 0 \quad (3)$$

where N indicates axial force, M indicates moment, and Q indicates shear force per unit width. The comma identifies differentiation w.r.t. the axis number after the comma. The superscript k identifies layer number. The difference in interfacial stresses between layers k and $(k-1)$ yield the stress imposed on each layer, which can be given by

$$n_2^k = \sigma_{2z}^{k-1}(x_2, c_k) - \sigma_{2z}^k(x_2, -c_k) \quad (4a)$$

$$m_2^k = \sigma_{2z}^{k-1}(x_2, c_k) + \sigma_{2z}^k(x_2, -c_k) \quad (4b)$$

$$q^k = \sigma_{zz}^{k-1}(x_2, c_k) - \sigma_{zz}^k(x_2, -c_k). \quad (4c)$$

For a beam-type plate all, derivatives with respect to X_1 are zero. The thickness of the k th ply is $2c^k$. The superscript k , which identifies the generic ply, will be dropped in the subsequent part for convenience.

During manufacturing, most microelectronic components are exposed to a thermal gradient rather than a homogeneous condition. Considering the thermal gradient across the laminated assembly to be $\Delta T = az + b$, the constitutive relations can be derived as follows:

$$\frac{N_i}{h} = -\bar{C}_{ij}b\alpha_j + \bar{C}_{i2}U_{2,2} + K_{ni}cn_{2,2} + K_{pi}p, \quad i, j = 1, 2 \quad (5a)$$

$$\frac{M_i}{I} = -\bar{C}_{ij}a\alpha_j - \bar{C}_{i2}W_{,22} + K_{mi}m_{2,2} + K_{qi}q/c \quad (5b)$$

$$\Phi_2 + W_{,2} = \frac{c^2}{2I}S_{44} \left(Q_2 - \frac{1}{3}cm_2 \right) \quad (5c)$$

where

$$K_{mi} = (3\bar{C}_{i2}S_{3j}\bar{C}_{j2}/\bar{C}_{22} - 2\bar{C}_{i2}S_{44} + 2\bar{C}_i)/20, \quad i, j = 1 \text{ and } 2$$

$$K_{qi} = (3\bar{C}_{i2}S_{3j}\bar{C}_{j2}/\bar{C}_{22} - 12\bar{C}_{i2}S_{44} + 12\bar{C}_i)/20$$

$$K_{ni} = (\bar{C}_{i2}S_{3j}\bar{C}_{j2}/\bar{C}_{22} + \bar{C}_{i2}S_{44} + 2\bar{C}_i)/12$$

$$K_{pi} = \bar{C}_i/2$$

$$p = \sigma_{zz}(x_2, c) + \sigma_{zz}(x_2, -c)$$

$$h = 2c, \quad I = 2c^3/3$$

$$\begin{aligned} \bar{C}_{11} &= C_{11} - \frac{C_{13}C_{31}}{C_{33}}, & \bar{C}_{12} &= C_{12} - \frac{C_{13}C_{32}}{C_{33}} \\ \bar{C}_{21} &= C_{21} - \frac{C_{23}C_{31}}{C_{33}}, & \bar{C}_{22} &= C_{22} - \frac{C_{23}C_{32}}{C_{33}} \\ \bar{C}_1 &= \frac{C_{13}}{C_{33}}, & \bar{C}_2 &= \frac{C_{23}}{C_{33}} \end{aligned} \quad (6)$$

where

- C_{ij} stiffness coefficients of orthotropic materials;
- α_j coefficient of thermal expansion of k th layer in direction j ;
- ΔT temperature field function, a and b are constants (assuming linear change in temperature);
- U, W displacement components in the x_2 and z directions, respectively, at $z = 0$ surface,
- Φ_2 the rotation of a normal to the reference surface ($z = 0$).

The solution of the differential equations given by the equilibrium equations and interfacial compatibility conditions (which is discussed extensively in Section III) for the classical plate theory yield the following stress and displacement distribution equations

$$\sigma_i = \frac{1}{h}N_i + \frac{1}{2h}K_i n_{2,2}(z^2 - c^2/3) + \frac{z}{I}M_i + \frac{1}{6I}K_i(cm_{2,2} + q)(z^3 - 3c^2z/5), \quad i, j = 1, 2 \quad (7a)$$

$$\sigma_{2z} = \frac{z}{h}n_2 + \frac{c}{6I}m_2(3z^2 - c^2) - \frac{1}{2I}Q_2(z^2 - c^2) \quad (7b)$$

$$\sigma_{zz} = \frac{1}{2}p - \frac{1}{2h}n_{2,2}(z^2 - c^2) + \frac{z}{h}q - \frac{1}{6I}(cm_{2,2} + q)(z^3 - c^2z) \quad (7c)$$

where

$$K_i = \bar{C}_{i2}S_{3j}\bar{c}_{2j}/\bar{C}_{22} + \bar{C}_{i2}S_{44} - \bar{C}_i, \quad i, j = 1, 2 \quad (8)$$

where

- σ_1 normal stress in the x_1 direction in any layer;
- σ_2 normal stress in the x_2 direction, in any layer;
- σ_{2z} shear stress in the $x_2 - z$ plane;
- σ_{zz} transverse normal stress in the thickness coordinate z direction, peeling stress

$$\begin{aligned} w &= W + S_{3j} \left(N_j \frac{z}{h} + M_j \frac{z^2}{2I} \right) \\ &+ S_{3j}K_j \frac{1}{6h}n_{2,2}(z^3 - c^2z) \\ &+ S_{3j}K_j \frac{cm_{2,2} + q}{6I}(z^4/4 - 3c^2z^2/10) \\ &+ S_{33} \left(\frac{z}{2}p + \frac{z^2}{2h}q \right) \\ &- S_{33} \frac{1}{6h}n_{2,2}(z^3 - 3c^2z) \\ &- S_{33} \frac{cm_{2,2} + q}{6I}(z^4/4 - c^2z^2/2) \\ &+ \left(\frac{1}{2}az^2 + bz \right) \alpha_z \quad j = 1, 2 \\ u_2 &= U_2 - zW_{,2} - S_{3j} \left(N_j \frac{z^2}{2h} + M_j \frac{z^3}{6I} \right)_{,2} \\ &- S_{3j}K_j \left\{ \frac{n_{2,22}}{6h}(z^4/4 - c^2z^2/2) \right. \\ &+ \left. \frac{cm_{2,22} + q_{,2}}{6I}(z^5/20 - c^2z^3/10) \right\} \\ &- S_{33} \left\{ \frac{z^2}{4}p_{,2} - \frac{1}{6h}n_{2,22}(z^4/4 - 3c^2z^2/2) \right. \\ &+ \left. \frac{z^3}{6h}q_{,2} - \frac{cm_{2,22} + q_{,2}}{6I}(z^5/20 - c^2z^3/6) \right\} \\ &+ S_{44} \left\{ \frac{z^2}{2h}n_2 + \frac{1}{6I}cm_2(z^3 - c^2z) \right. \\ &- \left. \frac{1}{6I}Q_2(z^3 - 3c^2z) \right\} \end{aligned} \quad (9a;b)$$

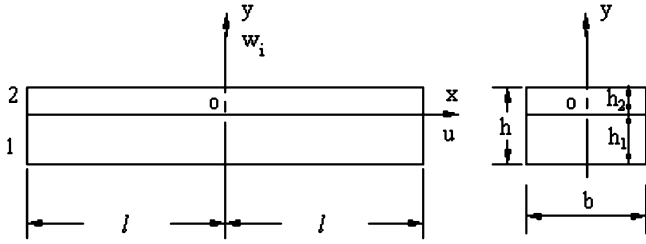


Fig. 2. Elongated bimaterial plate.

where w , u_2 are the displacement components in the z and x_2 coordinate directions, respectively.

III. COEFFICIENTS OF INTERFACIAL COMPLIANCES

The interfacial compliance concept was first put forward by Suhir [1]–[3], and the coefficient of interfacial compliance was given for the longitudinal direction in the beam. However, there was an error in Suhir's derivation of the coefficient of interfacial compliance for the longitudinal direction. The expansion of function $\cotanh u_k$ was inaccurate which led to a compliance coefficient that does not satisfy the differential equations. Afterwards, Suhir [4] reported the transverse interfacial compliance coefficient. Here, we correct Suhir's error and rederive the interfacial compliance coefficients based on more general case of orthotropic material properties and plate theory, rather than the beam theory used in Suhir's solution.

A. Transverse Interfacial Compliance Coefficient

Considering an elongated bimaterial plate as shown in Fig. 2, the displacement can be evaluated from Ribiere solution for a long-and-narrow strip Timoshenko and Goodier [6]

$$w_1(x) = -\frac{(1-\nu_1^2)h_1}{E_1}p(x) \quad (10a)$$

$$w_2(x) = \frac{(1-\nu_2^2)h_2}{E_2}p(x) \quad (10b)$$

where $w_1(x)$ and $w_2(x)$ are vertical deflections of the plate for the first layer and the second layer along the y direction, ν_1 and ν_2 are Poisson's ratios, h_1 and h_2 are the plate thicknesses, and $p(x)$ is the peeling stress at the interface.

Subtracting (10b) from (10a) leads to

$$w_1(x) = w_2(x) - \left[\frac{(1-\nu_1^2)h_1}{E_1} + \frac{(1-\nu_2^2)h_2}{E_2} \right] p(x). \quad (11)$$

If we define K_y as the transverse interfacial compliance

$$K_y = \frac{1}{\frac{(1-\nu_1^2)h_1}{E_1} + \frac{(1-\nu_2^2)h_2}{E_2}} \quad (12)$$

then (11) can be given as

$$w_1(x) = w_2(x) - \frac{p(x)}{K_y}. \quad (13)$$

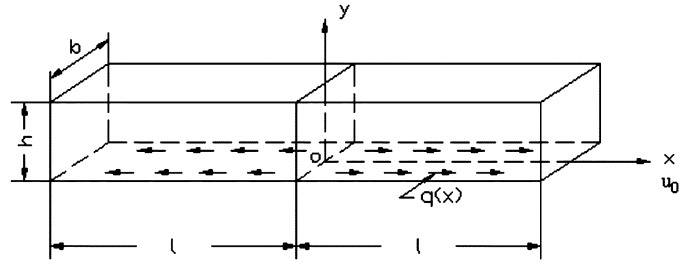


Fig. 3. Long-and-narrow strip subjected to shear loading.

B. Longitudinal Interfacial Compliance Coefficient

For a long-and-narrow strip under shear loading at the surface (Fig. 3), neglecting the bending contribution, the displacement along the x axis at the edge $y=0$ can be written as

$$u_0 = -\frac{1-\nu^2}{Ehb} \int_0^x Q(\xi)d\xi + Kq(x) \quad (14)$$

where E and ν are the elastic constants for the strip material, K is the interfacial compliance, h is the thickness of the strip, b is the plate width, $q(x)$ is the shear force per unit plate length, $Q(x)$ is the force at the x cross section and

$$Q(x) = \int_{-l}^x q(\xi)d\xi. \quad (15)$$

Expanding $q(x)$ to a harmonics $\sin \alpha_k x$ series leads to

$$q(x) = b\tau_0(x) = b \sum_k \alpha_k \gamma_k \sin \alpha_k x. \quad (16)$$

Substituting (16) into (15), and then into (14) yields

$$u_0(x) = \frac{1-\nu^2}{E} \sum_k \frac{\gamma_k}{u_k} \sin \alpha_k x + Kb \sum_k \alpha_k \gamma_k \sin \alpha_k x \quad (17)$$

On the other hand, the displacement along the x axis at the edge $y=0$ can also be obtained from the Ribiere solution for a long-and-narrow plate strip as follows:

$$u_0(x) = \frac{1}{4G} \sum_{k=1,3,5,\dots} \gamma_k [3-\nu - (1+\nu)u_k \cotanh u_k] \cotanh u_k + (1+\nu)u_k \sin \alpha_k x. \quad (18)$$

where

$$G = \frac{E}{2(1+\nu)}, \quad u_k = \alpha_k h = \frac{k\pi h}{2l}$$

$$\gamma_k = \frac{2}{\alpha_k l} \int_0^l \tau_0(x) \sin \alpha_k x dx.$$

Comparing (18) with (17), we find that

$$K = \frac{\sum_k \gamma_k N(u_k) \sin \alpha_k x}{Eb \sum_k \alpha_k \gamma_k \sin \alpha_k x} \quad (19)$$

where $N(u_k) = (1 + \nu/2)[(3 - \nu - (1 + \nu)u_k \cothanh u_k) \cothanh u_k + (1 + \nu)u_k - (2(1 - \nu)/u_k)]$. For sufficiently small (h/l) ratios (say, $(h/l) < 0.2$, which is usually the case in microelectronic packaging), we have

$$\begin{aligned} \cothanh u_k &= \frac{\cosh u_k}{\sinh u_k} = \frac{e^{u_k} + e^{-u_k}}{e^{u_k} - e^{-u_k}} \\ &= \frac{1 + u_k + \frac{u_k^2}{2} + \frac{u_k^3}{6} + 1 - u_k + \frac{u_k^2}{2} - \frac{u_k^3}{6}}{1 + u_k + \frac{u_k^2}{2} + \frac{u_k^3}{6} - 1 + u_k - \frac{u_k^2}{2} + \frac{u_k^3}{6}} \\ &= \frac{2 + u_k^2}{2u_k + \frac{u_k^3}{3}}. \end{aligned}$$

Neglecting the third order term u_k^3 , then

$$\begin{aligned} \cothanh u_k &= \frac{1}{u_k} + \frac{u_k}{2} \\ N(u_k) &= \frac{(1 + \nu)(3 - \nu)}{4} u_k = \frac{(1 + \nu)(3 - \nu)}{4} \alpha_k h. \end{aligned} \tag{20}$$

Substituting (20) into (19), we get the simple formula for the longitudinal interfacial compliance coefficient as

$$K = \frac{(1 + \nu)(3 - \nu)h}{4b}. \tag{21}$$

For an elongated bimaterial plate shown in Fig. 2, neglecting the bending contribution, the displacements at the interface ($y = 0$) $u_1(x)$ and $u_2(x)$ can be evaluated as

$$u_1(x) = -\frac{1 - \nu_1^2}{E_1 h_1} \int_0^x Q(\xi) d\xi + \frac{(1 + \nu_1)(3 - \nu_1)h_1}{4} \tau(x) \tag{22a}$$

$$u_2(x) = \frac{1 - \nu_2^2}{E_2 h_2} \int_0^x Q(\xi) d\xi - \frac{(1 + \nu_2)(3 - \nu_2)h_2}{4} \tau(x) \tag{22b}$$

where $\tau(x)$ is the shear stress at the interface.

Subtracting (22b) from (22a) yields

$$\begin{aligned} u_1(x) = u_2(x) - \left(\frac{1 - \nu_1^2}{E_1 h_1} + \frac{1 - \nu_2^2}{E_2 h_2} \right) \int_0^x Q(\xi) d\xi \\ + \left[\frac{(1 + \nu_1)(3 - \nu_1)h_1}{4} + \frac{(1 + \nu_2)(3 - \nu_2)h_2}{4} \right] \tau(x). \end{aligned} \tag{23}$$

Say

$$u_1(x) = u_2(x) - \left(\frac{1 - \nu_1^2}{E_1 h_1} + \frac{1 - \nu_2^2}{E_2 h_2} \right) \times \int_0^x Q(\xi) d\xi + \frac{\tau(x)}{K_x} \tag{24}$$

where K_x is the longitudinal interfacial compliance, where it is given by

$$K_x = \frac{1}{\frac{(1 + \nu_1)(3 - \nu_1)h_1}{4} + \frac{(1 + \nu_2)(3 - \nu_2)h_2}{4}}. \tag{25}$$

IV. CASE STUDY—A THREE-LAYERED MICROELECTRONIC STRUCTURE

In order to investigate the influence of interfacial compliances on thermomechanical stresses in microelectronics packaging, a three-layered structure with dimensions common to microelec-

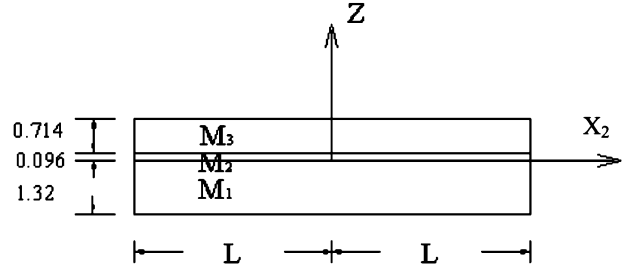


Fig. 4. Idealized model geometry (dimensions are given in Table I).

tronics packaging is considered. Fig. 4 shows the idealized geometry used in this study. The first layer is bismaleimide-triazine (BT) and the third layer is silicon. To illustrate the influence of interfacial compliances, we consider two different types bonding materials, which make the middle layers in Fig. 4. One is eutectic Pb/Sn solder layer as a stiff bonding layer and the other is epoxy layer as a compliant bonding material. During the manufacturing process, the microelectronic packaging modules usually experience a high temperature gradient of approximately 400 °C. In this paper, the microelectronic structure is subjected to uniform temperature change of $\Delta T = 400$ °C.

Considering the interfacial compliances, the compatibility of the displacement field is imposed at the interfaces as follows:

$$u_2^1 \left(x_2, \frac{h_1}{2} \right) = u_2^2 \left(x_2, -\frac{h_2}{2} \right) + \frac{\sigma_{zz}^1}{K_{x1}} \tag{26a}$$

$$u_2^2 \left(x_2, \frac{h_2}{2} \right) = u_2^3 \left(x_2, -\frac{h_3}{2} \right) + \frac{\sigma_{zz}^2}{K_{x2}} \tag{26b}$$

$$w^1 \left(x_2, \frac{h_1}{2} \right) = w^2 \left(x_2, -\frac{h_2}{2} \right) - \frac{\sigma_{zz}^1}{K_{y1}} \tag{26c}$$

$$w^2 \left(x_2, \frac{h_2}{2} \right) = w^3 \left(x_2, -\frac{h_3}{2} \right) - \frac{\sigma_{zz}^2}{K_{y2}} \tag{26d}$$

where

- σ_{zz}^1 peeling stress at interface 1;
- σ_{zz}^2 peeling stress at interface 2;
- σ_{zz}^1 shear stress at interface 1;
- σ_{zz}^2 shear stress at interface 2;
- $K_{x1}, K_{x2}, K_{y1}, K_{y2}$ orthotropic interfacial compliances, and according to the derivation given in Section III, they can be evaluated as follows:

$$\begin{aligned} K_{x1} &= \frac{1}{\frac{(1 + \nu_{231})(3 - \nu_{231})h_1}{4E_{21}} + \frac{(1 + \nu_{232})(3 - \nu_{232})h_2}{8E_{22}}} \\ K_{y1} &= \frac{1}{\frac{(1 - \nu_{231}^2)h_1}{E_{31}} + \frac{(1 - \nu_{232}^2)h_2}{2E_{32}}} \\ K_{x2} &= \frac{1}{\frac{(1 + \nu_{232})(3 - \nu_{2312})h_2}{8E_{22}} + \frac{(1 + \nu_{233})(3 - \nu_{233})h_3}{4E_{23}}} \\ K_{y2} &= \frac{1}{\frac{(1 - \nu_{232}^2)h_2}{2E_{32}} + \frac{(1 - \nu_{233}^2)h_3}{E_{33}}} \end{aligned} \tag{27}$$

where E_{21}, E_{31} indicate the Young's modulus E_2 and E_3 for the first layer, respectively. E_{22}, E_{32} indicate the Young's modulus E_2 and E_3 for the second layer, respectively. E_{23}, E_{33} indicate the Young's modulus E_2 and E_3 for the third layer, re-

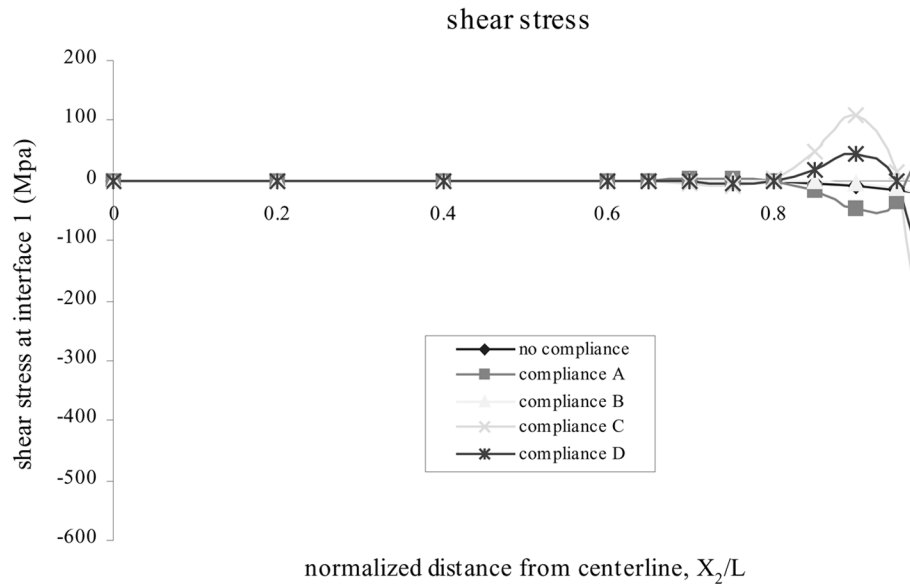


Fig. 5. Comparison of shear stress at interface 1 for no compliance, and A, B, C, and D compliance scenarios.

spectively. $\nu_{231}, \nu_{232}, \nu_{233}$ indicate the Poisson ratio ν_{23} for the first, second, and third layer, respectively. h_1, h_2, h_3 indicate the thickness for the first, second, and third layer, respectively.

After introduction of the boundary conditions, using a hyperbolic differential equation solution method, we can obtain the analytical solution which detail are given by Wen and Basaran in [9].

To investigate the influence of interfacial compliance on the thermomechanical stresses, we assume four cases of compliant interface configurations as follows.

Compliance A: Considering the compliances in x_2 and z directions at interface 1 and neglecting the corresponding compliances at interface 2.

Compliance B: Considering the compliances in x_2 and z directions at interface 2 and neglecting the corresponding compliances at interface 1.

Compliance C: Considering the compliances in x_2 and z directions at both interface 1 and interface 2.

Compliance D: Considering the compliances in x_2 direction at both interface 1 and interface 2 and neglecting the corresponding compliances in z direction.

Each one of these cases corresponds to certain potential next-generation microelectronic package designs.

V. RESULTS AND DISCUSSION

A. Eutectic Pb/Sn Solder Layer as a Bonding Material

Table I shows the orthotropic material properties and the dimensions for the structure, where solder is the bonding material.

Figs. 5 and 6 show the shear stress distribution along interfaces 1 and 2 for no compliance, and compliance cases A, B, C, and D. Compared to the shear stresses with no compliance, -24.2 MPa at interface 1 and -110.5 MPa at interface 2, and compliance cases A, B, C, and D yield increasing shear stress values, $153.5, -27.6, -550.3,$ and -289.8 MPa at interface 1 and $-700.9, -554.4, -536.5,$ and -355.5 MPa at interface 2, respectively. Introducing interfacial compliance increases shear

TABLE I
MATERIAL PROPERTIES FOR THE STRUCTURE WITH SOLDER LAYER

	M ₁ (BT)	M ₂ (Pb/Sn solder)	M ₃ (silicon)
E ₁ (Gpa)	17.5	24.3	112
E ₂ (Gpa)	10.4	24.3	148
E ₃ (Gpa)	4.7	24.3	168
G ₁₂ (Gpa)	3.54	9.2	46.2
G ₁₃ (Gpa)	9.04	9.2	33.2
G ₂₃ (Gpa)	1.58	9.2	51.7
ν_{12}	0.32	0.32	0.28
ν_{13}	0.32	0.32	0.28
ν_{23}	0.32	0.32	0.28
α_1 (e-6/ $^{\circ}$ C)	16	24.7	3
α_2 (e-6/ $^{\circ}$ C)	16	24.7	3
α_3 (e-6/ $^{\circ}$ C)	16	24.7	3
h (mm)	1.32	0.096	0.714
2L(mm)	20.5		

stress level both at interface 1 and interface 2. Figs. 7 and 8 show the peeling stress distribution along interface 1 and interface 2 for no compliance, and compliance cases A, B, C, and D, respectively. The maximum peeling stress values for no compliance, and compliance cases A, B, C, and D are $147.96, -10.4, -76.5, 48.2,$ and 122.6 MPa at interface 1 and $-77.4, 228.92, 407.4, 251.5,$ and -242.9 MPa at interface 2, respectively. Comparing the peeling stress values at interface 1 and interface 2 for no compliance, and A, B, C, and D compliance scenarios indicates that introducing interfacial compliance lowers the peeling stress level at interface 1 but increase the peeling stress values at interface 2.

The axial normal stress distributions in the BT layer and silicon layer are shown in Figs. 9 and 10. Compared to the axial normal stresses with no compliance, -15.7 MPa in BT layer and 62.7 MPa in silicon layer, compliance cases C and D yield stress values much larger, -84.5 MPa, -41.9 MPa in the BT layer and 174.9 and 111.2 MPa in the silicon layer, respectively. However, compliance scenarios A and B only increase stress values a little

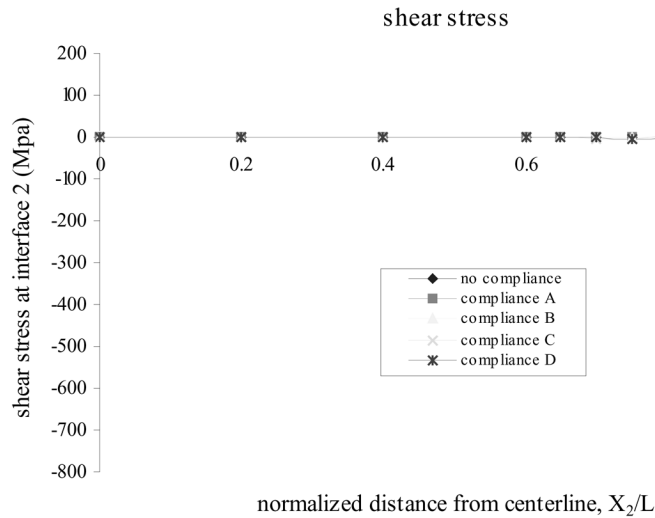


Fig. 6. Comparison of shear stress at interface 2 for no compliance, and A, B, C, and D compliance scenarios.

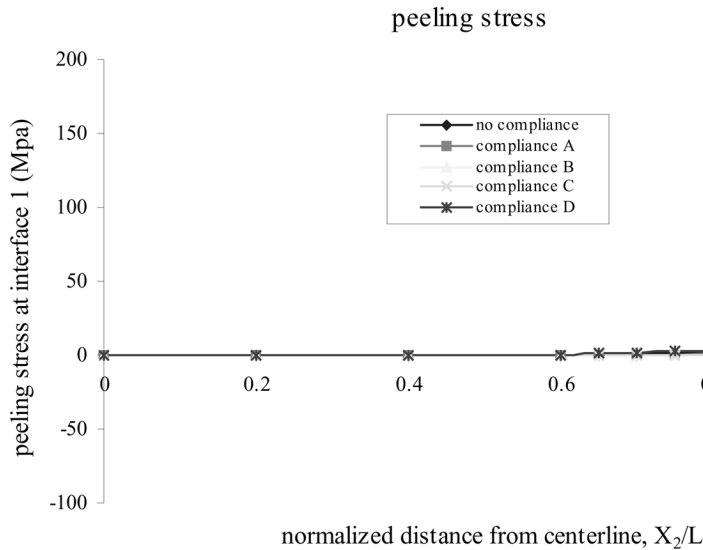


Fig. 7. Comparison of peeling stress at interface 1 for no compliance, and A, B, C, and D compliance scenarios.

bit, 17.3 and -15.76 MPa in the BT layer and 65.8 and 70.2 MPa in the silicon layer, respectively. Again having compliant interface increases the axial stresses in the layers. Figs. 9 and 10 show that the axial normal stress values in the BT and the silicon layers are almost the same from $x_2/L = 0$ to $x_2/L = 0.7$ for no compliance, and compliance cases A, B, C, and D. It should be pointed out that there is a jump near the free edge of the axial normal stress value in the BT layer for compliance cases A, C, and D and in the silicon layer for compliance cases B, C, and D. But there is no such jump in the BT layer for compliance B, in the silicon layer for compliance A, and for no compliance case. The jump is due to interfacial compliance. Compared to BT material solder is stiffer. Hence, on the BT side of the interface, in case B, there is no compliance. This is also evident that scenario C introducing the compliance in both x_2 and y directions results in much more jump in stress than scenario D introducing the compliance only in x_2 direction. In the case of the silicon layer, there is no jump in shear stresses near the free

edge as much when there is no interfacial compliance on the silicon side of the solder layer.

B. Adhesive Epoxy Layer as a Bonding Material (Die Attach)

In this case, it is assumed that the second layer is epoxy with soft interfaces relative to BT and silicon.

Due to space limitations, figures are shown, yet the results are discussed in detail. The shear stress distribution along interfaces 1 and 2 for no compliance, and compliance cases A, B, C, and D, respectively, were investigated. Compared to the shear stresses with no compliances, -13.8 MPa at interface 1 and -22.5 MPa at interface 2, compliances A and D yield higher shear stress values, 24.5 and -17.3 MPa at interface 1 and -77.2 and -40.9 MPa at interface 2, respectively. Compliance C yields a higher shear stress value -27.4 MPa at interface 1 and a lower shear stress value -22.1 MPa at interface 2, and compliance B yields a lower shear stress value, 5.99 MPa at interface 1 and -9.5 MPa at interface 2. The peeling stress distribution along interface 1

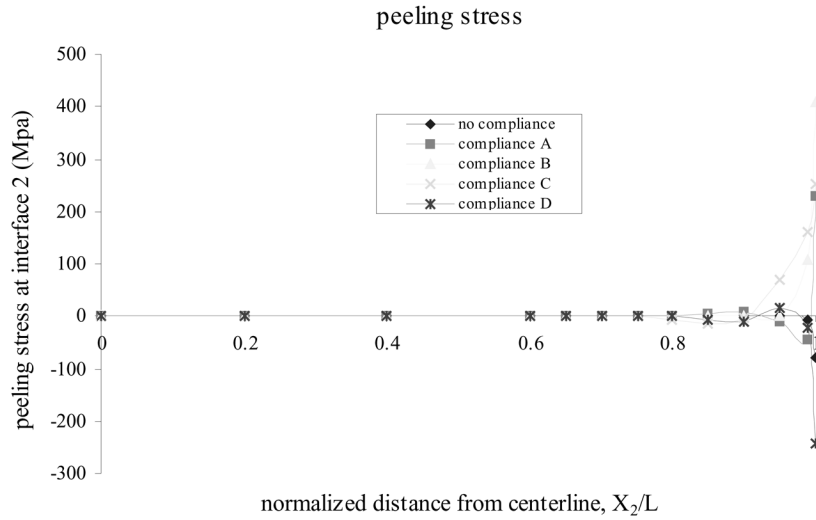


Fig. 8. Comparison of peeling stress at interface 2 for no compliance, and A, B, C, and D compliance scenarios.

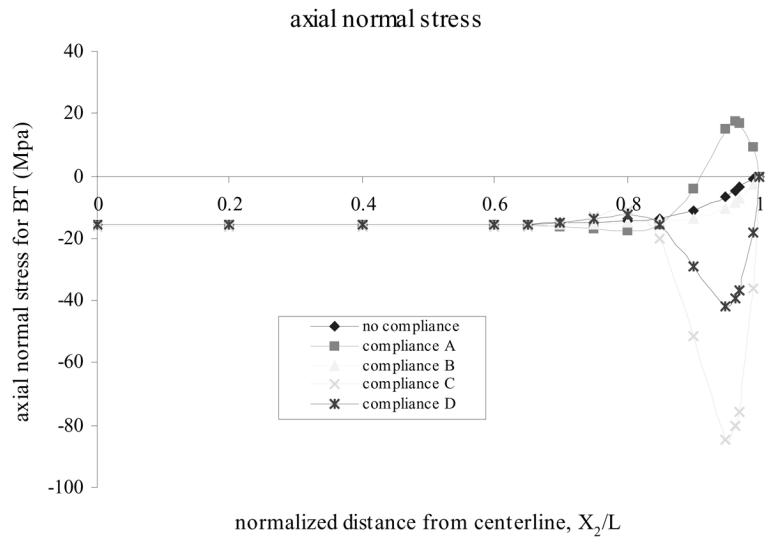


Fig. 9. Comparison of axial normal stress in the bottom side of BT layer for no compliance, and A, B, C, and D compliance scenarios.

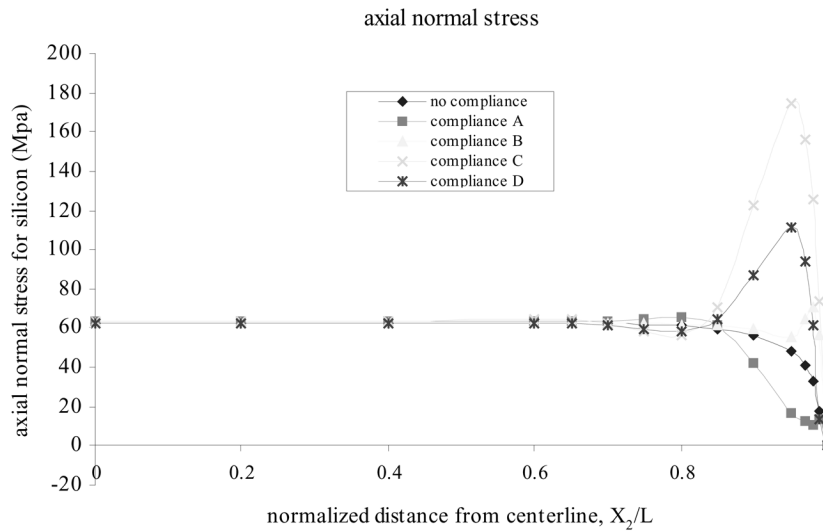


Fig. 10. Comparison of axial normal stress in the top side of silicon layer for no compliance, and A, B, C, and D compliance scenarios.

and interface 2 for no compliance, and for cases A, B, C, and D were also investigated. The maximum peeling stress values for no compliance, and compliance cases A, B, C, and D are -10.5 , 96.97 MPa, 19.4 MPa, 26.5 MPa, and -13.8 MPa at interface 1 and -20.2 , 26.3 , 13.5 , -37.8 , and -41.3 MPa at interface 2, respectively. Comparing the peeling stresses at interface 1 and interface 2 for no compliances, and cases A, B, C, and D indicates that introducing interfacial compliances can increase the peeling stress level at both interface 1 and interface 2, except for the case B, lowers the peeling stress at interface 2.

Compared to compliance cases A, C, and D, compliance case B significantly reduces the interfacial stress level, except for the peeling stress at interface 1. This is due to the larger stiffness difference between the silicon and the epoxy layer at interface 2 compared to the stiffness difference between the BT and the epoxy layer at interface 1. Shear stress at interface 1 is reduced by 56.6%, shear stress at interface 2 is reduced by 57.8%, peeling stress at interface 2 is reduced by 33.2%, axial normal stress in the BT layer is reduced by 90.6%, and axial normal stress in silicon layer is reduced by 96.8%.

VI. CONCLUSION

The analytical method proposed in this paper provides an accurate and quick method to obtain stresses in a multilayered orthotropic structure with interfacial compliances. Interfacial compliances have significant influence on thermomechanical stresses in multilayered microelectronics. Comparing the above two cases with a stiffer solder adhesive layer and a softer epoxy adhesive layer indicates that a softer adhesive layer can significantly lower the interfacial shear stress level and the axial normal stress in the bonded layers. A high shear stress and peeling stress level are usually responsible for the delamination failure in microelectronic devices. And the die crack often results from the high normal stress level in the silicon layer. Using a softer adhesive layer can effectively increase the yield during manufacturing semiconductor devices. The interfacial compliances must be taken into account in structural analysis of microelectronic packaging, where reducing the stresses in silicon layer is a big concern to increase production yield.

REFERENCES

- [1] E. Suhir, "Stresses in adhesively bonded bi-material assemblies used in electronic packaging," in *Proc. Elect. Pack. Mat. Science-II, MRS Symp.*, 1986, pp. 133–138.
- [2] —, "Stresses in bi-metal thermostats," *Trans. ASME J. Appl. Mech.*, vol. 53, no. 3, pp. 657–660, 1986.
- [3] —, "Calculated thermally induced stresses in adhesively bonded and soldered assemblies," in *Proc. Int. Symp. Microelect.*, 1986, pp. 383–392.
- [4] E. Suhir, "Interfacial stresses in bimetal thermostats," *ASME J. Appl. Mech.*, vol. 56, pp. 595–600, 1989.
- [5] S. Timoshenko, "Analysis of bi-metal thermostats," *J. Optic. Soc. Amer.*, vol. 11, pp. 233–255, 1925.
- [6] S. P. Timoshenko and J. N. Goodier, *Theory of Elasticity*, 3rd ed. New York: McGraw-Hill, 1970.
- [7] Y. J. Wen and C. Basaran, "Thermal stress analysis of multilayered microelectronic packaging," *ASME J. of Electronic Packaging*, vol. 125, pp. 134–138, 2003.
- [8] —, "Analysis of multilayered microelectronic packaging under uniformly distributed loading," *Int. J. Solids Structures*, vol. 40, no. 13–14, pp. 3331–3345, 2003.
- [9] Y. J. Wen and C. Basaran, "An analytical model for thermal stress analysis of multilayered microelectronic packaging," *Mech. f Mater.*, vol. 36, pp. 369–385, 2004.

Cemal Basaran received the M.S. degree in civil engineering from the Massachusetts Institute of Technology, Cambridge, and the Ph.D. degree in engineering mechanics from the University of Arizona, Tucson.

He is a Professor and Director of the Electronic Packaging Laboratory at the State University of New York, Buffalo. He specializes in experimental and computational damage mechanics of micro- and nanoelectronics packaging under thermomechanical, high current density and high-temperature gradient loads. He is currently working on electromigration and thermomigration in nano and power electronics packaging projects funded by the U.S. Navy Office of Naval Research. He has authored and coauthored more than 120 publications in the field of electronics packaging reliability, moiré interferometry (which has 27.5-nm resolution), and thermodynamics-based damage mechanics.

Prof. Basaran is the 1997 recipient of the Department of Defense Office of Naval Research Young Investigator Award.

Yujun Wen received the M.S. degree in civil engineering from Tongji University, Shanghai, China, and the Ph.D. degree in computational mechanics from the State University of New York, Buffalo.

He is a Senior Supervisor at Shanghai Shentong Holdings Company, Ltd., Shanghai, China. He specializes in moiré interferometry inspection and analytical methods for thermomechanical analysis of microelectronic packaging.